Am J Nucl Med Mol Imaging 2015;5(3):259-269
www.ajnmmi.us /ISSN:2160-8407/ajnmmi0007362

Original Article

Dosimetry of [^{68}Ga]Ga-DO3A-VS-Cys^{40}-Exendin-4 in rodents, pigs, non-human primates and human - repeated scanning in human is possible

Ram Kumar Selvaraju[1*], Thomas N Bulenga[1*], Daniel Espes[2,5], Mark Lubberink[3,4], Jens Sörensen[4], Barbro Eriksson[5], Sergio Estrada[1], Irina Velikyan[1,3,4], Olof Eriksson[1]

[1]Department of Medicinal Chemistry, Preclinical PET Platform, Uppsala University, Uppsala, Sweden; [2]Department of Medical Cell Biology, Uppsala University, Uppsala, Sweden; [3]Department of Surgical Sciences, Radiology, Uppsala University, Uppsala, Sweden; [4]PET Centre, Centre for Medical Imaging, Uppsala University Hospital, Uppsala, Sweden; [5]Department of Medical Sciences, Uppsala University, Uppsala, Sweden. [*]Equal contributors.

Received February 26, 2014; Accepted March 10, 2015; Epub February 15, 2015; Published March 1, 2015

Abstract: Quantitative PET imaging with [^{68}Ga]Ga-DO3A-VS-Cys^{40}-Exendin-4 has potential use in diabetes and cancer. However, the radiation dose to the kidneys has been a concern for the possibility of repeated imaging studies in humans. Therefore, we investigated the dosimetry of [^{68}Ga]Ga-DO3A-VS-Cys^{40}-Exendin-4 based on the biodistribution data in rats, pigs, non-human primates (NHP) and a human.Organ distribution of [^{68}Ga]Ga-DO3A-VS-Cys^{40}-Exendin-4 in rats (Male Lewis; n=12; 30, 60, and 80 min) was measured ex vivo. The dynamic uptake of [^{68}Ga]Ga-DO3A-VS-Cys^{40}-Exendin-4 in the abdomen was assessed by PET/CT scanning of pigs (male; n = 4, 0-60 min), NHP (Female; cynomolgus; n=3; 0-90 min), and human (female; n=1; 0-40, 100, 120 min).The organ distribution data in each species were extrapolated to those of a human, assuming similar distribution between the species. Residence times were assessed by trapezoidal approximation of the kinetic data. Organ doses (mGy/MBq) and the whole body effective dose (mSv/MBq), was extrapolated by using the OLINDA/EXM 1.1 software. The extrapolated human whole body effective dose was 0.017 ± 0.004 (rats), 0.014 ± 0.004 (pigs), 0.017 ± 0.004 (NHP), and 0.016 (human) mSv/MBq. The absorbed dose to the kidneys was limiting:0.33 ± 0.06 (rats), 0.28±0.05 (pigs), 0.65 ± 0.11 (NHP), and 0.28 (human) mGy/MBq, which corresponded to the maximum yearly administered amounts of 455 (rat), 536 (pig), 231 (NHP), and 536 (human) MBq before reaching the yearly kidney limiting dose of 150 mGy. More than 200 MBq of [^{68}Ga]Ga-DO3A-VS-Cys^{40}-Exendin-4 can be administered yearly in a human, allowing for repeated (2-4 times) scanning. This potentially enables longitudinal clinical PET imaging studies of the GLP-1R in the pancreas, transplanted islets, or insulinoma.

Keywords: Dosimetry, [^{68}Ga]Ga-DO3A-VS-Cys^{40}-Exendin-4, GLP-1R, PET, islet imaging, insulinoma

Introduction

The estimation of the absorbed doses in different organs of patients for any new developed radiopharmaceutical is indispensable. The development of radionuclide-based diagnostics and subsequent targeted radiation therapy has triggered the importance of the internal dosimetry information to estimate the radiation risks versus the benefits in nuclear medicine [1, 2]. Furthermore, the dosimetry information is a significant criterion for approving new radiopharmaceuticals for clinical applications.

[^{68}Ga]Ga-DO3A-VS-Cys^{40}-Exendin-4 is reported to be a promising imaging candidate to target the glucagon like peptide-1 receptor (GLP-1R), which is highly expressed by the pancreatic β-cells and insulinoma tumors. Its radio-synthesis and subsequent biodistribution characteristics *in vivo* have been described in different species models [3-6].

[^{68}Ga]Ga-DO3A-VS-Cys^{40}-Exendin-4 can serve two main purposes in the clinical setting. First, it can help in understanding the etiology and progression of diabetes. In fact, very little is known regarding the β-cell mass (BCM) during the progression of diabetes in humans and what is known is largely based on morphological studies of the pancreas post mortem. The

Table 1. Summary of species models and exendin-4 peptide dose used in the studies

Animal Model	n	Weight (kg)	Peptide dose (μg/kg)	Activity (MBq)	Time points (min)
Rat	12	0.36 ± 0.01	0.1	3.03 ± 0.79	30, 60, 80
Pig	4	31.0 ± 2.5	0.021 ± 0.003	7.45 ± 2.55	0-60
Non-human primate	3	7.33 ± 1.70	0.037 ± 0.023	1.51 ± 1.15	0-90
Human	1	115	0.17	101.2	0-40, 100, 120

imaging and quantification of BCM *in vivo* would help to longitudinally assess the progression of Type 1 and Type 2 Diabetes (T1D/ T2D),which normally rely on the WHO criteria in regard to diabetic symptoms expressed by the patients [7, 8]. Most importantly, it would be an indispensable tool for assessing the efficacy of novel anti-diabetic drugs aiming to replace, proliferate, or protect the β-cells and visualize viable transplanted islets of Langerhans. Moreover, [^{68}Ga]Ga-DO3A-VS-Cys^{40}-Exendin-4 can potentially be used as a GLP-1R target engaging a biomarker in the drug development of novel GLP-1 agonists.

Another potential use for [^{68}Ga]Ga-DO3A-VS-Cys^{40}-Exendin-4 is in the non-invasive imaging of insulinoma, a form of pancreatic endocrine tumor that causes hyperinsulinamic hypoglycemia in adults. Such tumors can be localized with [^{68}Ga]Ga-DO3A-VS-Cys^{40}-Exendin-4 due to their overexpression of GLP-1R [9]. [^{68}Ga]Ga-DO3A-VS-Cys^{40}-Exendin-4 may replace the regular diagnosis methods for localizing insulinoma such as [^{11}C]5-HTP-PET, magnetic resonance imaging (MRI), computed tomography (CT), or endoscopic ultrasound. The small size of many of the insulinoma metastasis (< 2 mm) has limited the use of conventional methods to localize the tumors based on their sensitivity and resolution. Other methods such as angiography, intra-arterial calcium stimulation, and venous sampling (ASVS) have improved the sensitivity but can cause complications due to their invasiveness. Recently, insulinoma has also been localized by targeting the somatostatin receptor by PET and SPECT. However, somatostatin receptor expression, in contrast to GLP-1R, is low in benign insulinoma (around 90% of all insulinoma), which limits the applications of somatostatin imaging analogs [10].

Due to the renal excretion of [^{68}Ga]Ga-DO3A-VS-Cys^{40}-Exendin-4 and the extensive intracellular retention of radioactivity in the kidney cortex, there have been concerns that the renal radiation dose might be too high for allowing repeated imaging in humans.

Therefore, we estimated the human dosimetry of this novel tracer extrapolated from the different species, namely, rat, pig, non-human primate (NHP), as well as from a case study reported on an insulinoma patient, to provide information of the dose distribution to normal organs. The dosimetry was calculated by the OLINDA/EXM 1.1 software, which uses different phantoms for extrapolation of dose estimations to humans [11]. In nuclear medicine, most of the attention has been paid to monitoring the absorbed doses to tumors for the optimization of therapy planning. However, with the increased use of PET and SPECT in the non-oncological setting, dosimetry is increasingly important, since even the low radioactivity associated with the diagnostic examinations could potentially be harmful to healthy tissue after repeated imaging examinations.

Material and methods

Radiochemistry

[^{68}Ga]Ga-DO3A-VS-Cys^{40}-Exendin-4 was synthesized in good manufacturing practice-compliant production and with quality control as previously described [3-6].

The production of the tracer for the experiments on the different species was accomplished within 1 hour, using the generator eluate fractionation method [12] with purification of the final product [13]. A sample in each batch was analyzed for the determination of identity, radiochemical and chemical purity, pH, estimation of the peptide content, as well as control of sterility and endotoxins.

Biodistribution of [^{68}Ga]Ga-DO3A-VS-Cys^{40}-exendin-4 in different animal models and human

The data from these studies have been published previously and are briefly summarized and compared herein [3, 4]. The amount of the administered peptide was less than 0.2 μg/kg (**Table 1**) in all of the species in order to avoid

pharmacological side effects and partial receptor saturation.

Biodistribution of [^{68}Ga]Ga-DO3A-VS-Cys^{40}-Exendin-4 in rats was measured by post mortem organ distribution. The dynamic uptake of [^{68}Ga]Ga-DO3A-VS-Cys^{40}-Exendin-4 in the abdomen of pigs, NHP, and human was assessed by PET/CT scanning.

Ex vivo organ distribution in rats: Lewis rats (male; n=12; 355.5 ± 13.1 g) were used in the study. The tracer was injected in the sedated animals (anesthesia, 3.5% isoflurane in 50%/50% medical oxygen/air at 450 mL/min) via the tail vein as a bolus of approximately 1 MBq, corresponding to 0.1 μg/kg of peptide. The animals were allowed to awaken immediately after the tracer administration and were sacrificed (with CO_2) at 30 min (n=2), 60 min (n=5), and 80 min (n=5) post injection time. The organs were resected and weighed, the radioactivity was measured in a well counter (Uppsala Imanet AB, Uppsala Sweden), and the tracer uptake in the organs was presented as a standardized uptake value (SUV).

Tracer kinetics analysed by PET-CT in pigs, non-human primate and human: The subject handling and anesthesia procedures have already been reported [3-5]. The pigs, NHP, and human were positioned in the Discovery ST PET/CT (GE Healthcare) with the abdomen in the center of the field of view, assisted with a low-dose CT scout view (140 kV, 10 mAs). The CT scans at 140 kV and 10-80 mAs were acquired for attenuation correction.

Forty-day old high-health herd-certified male pigs (Yorkshire x Swedish Landrace x Hampshire, SLU, Sweden) from the same litter (n=4), weighing 31.0 ± 2.5 kg, were examined by PET/CT. The animals were then injected intravenously with 8.08 ± 3.83 MBq, corresponding to 0.025 ± 0.01 μg/kg peptide of [^{68}Ga]Ga-DO3A-VS-Cys^{40}-Exendin-4, followed by dynamic PET scans of 30 frames for 60 min (12 × 10 s, 6 × 30 s, 5 × 120, 5 × 300 s, and 2 × 600 s) in the same position. Two of the animals were examined by multi-bed scans (five partly overlapping bed positions), following the dynamic baseline to investigate the whole body biodistribution. The PET data was acquired during 4 minutes for each bed position. Attenuation correction and morphological CT were obtained in the same manner as for the dynamic scan.

Healthy cynomolgus monkeys (female; n=3; 7.33 ± 1.70 kg) that were scanned at baseline dose were used in this investigation. The animals were injected with approximately 0.2 MBq/kg, corresponding to (0.04 ± 0.02) μg/kg of [^{68}Ga]Ga-DO3A-VS-Cys^{40}-Exendin-4. PET scans for 90 min were performed with 33 frames (12 × 10 s, 6 × 30 s, 5 × 120 s, 5 × 300 s, and 5 × 600 s). Immediately after the abdominal dynamic scan, the animals were examined with a multi-bed scan (3 or 4 partly overlapping bed positions) to cover the entire body. PET data were acquired for 5 min in each bed position. Attenuation correction and morphologic CT were accomplished in the same manner as for the dynamic scan.

A female patient (35 yr, 115 kg), who presented with severe chronic hypoglycemia, was admitted to the Uppsala University Hospital in Sweden, and her case report has been published [5]. However, the detailed biodistribution and kinetic data for this patient has not been previously published. The patient was intravenously injected with 0.88 MBq/kg, equivalent to 0.17 μg/kg of [^{68}Ga]Ga-DO3A-VS-Cys^{40}-Exendin-4 prior to the dynamic PET examinations over the liver and the pancreas for 40 minutes. This was followed by a whole body CT examination for attenuation correction and multi-bed whole body PET scans (4 min acquisition per bed position) at 100 and 120 minutes after injection.

PET-CT image reconstruction and analysis: All PET-CT 3-D image acquisition was performed by iterative OSEM VUEPOINT algorithm (4 mm Hann filter, 2 iteration, 21 subsets) into 128 × 128 matrix with pixel size 3.9 × 3.9 × 3.27 mm. Data analysis was performed by PMOD v3.508 (PMOD Technologies Ltd., Zurich, Switzerland). Regions of interest (ROIs) were created on the trans-axial CT slices. Entire organs were delineated on the sequential slices and combined into volumes of interest (VOIs). Mean VOI values for each time frame were used to calculate the SUVs normalized for body weight.

Ex vivo autoradiography of pancreas in rat

Sprague-Dawley (n=4; male; 338.5 ± 16.7 g) were administered 0.61 ± 0.1 MBq, corresponding to peptide mass of 0.1 μg/kg. The animals were euthanized by CO_2, 60 min p.i. The pancreas from the animals were removed post mortem, immediately frozen, and sectioned by

a microtome (Microm 560 cryostat, Cellab NordiaAB, Sweden) into 20 μm sections and placed upon object glasses. The object glasses from each animal were exposed to SR (Super Resolution) storage phosphor screens (PerkinElmer, Downers Grove, IL, USA), for 2 hr. The plates were scanned using a Cyclone plus phosphor imager (PerkinElmer, Model no. C4-31200, Downers Grove, IL, USA).

The pancreatic sections were immediately re-frozen and later thawed and stained for insulin by the immune fluorescence method (IF). The sections were fixed in ice-cold acetone for 10 minutes and then washed in PBS for 3 minutes, followed by incubation with DAKO Serum free protein block (Agilent Technologies, Glostrup, Denmark) for 30 minutes. The sections were then incubated over night at 4°C in the insulin primary antibody (Insulin A, Santa Cruz, SC-7839, goat-polyclonal (1:100) followed by wash in PBS (3 × 3 minutes). Slides were then incubated with secondary antibody Alexafluor 555 (Invitrogen, Carlsbad, CA, USA; donkey anti-goat; dilution 1:1000) for 60 minutes in a humidified dark chamber, again followed by washing PBS (3 × 3 minutes). ProLong ® Gold Antifade reagent (Life Technologies, Rockville, MD, USA) was used for mounting slides. Tile scan images were acquired with a Zeiss LSM780 confocal microscope at 10 × magnification.

The autoradiograms and the IF stains were co-registered and analyzed using Image J 1.48 v (National Institutes of Health, Bethesda, MD, USA).Manual ROIs were drawn on the regions of high radioactive signal density (assumed to correspond to islets of Langerhans) and within the regions with weak radioactivity signal (exocrine tissue). The overall phosphor image plate background was also assessed and subtracted from all data samples. The hotspot-to-exocrine uptake was expressed as a ratio for each analyzed section. Several sections (more than 3) from each animal were analyzed in this fashion.

Dosimetry

Residence time calculation: The assessment of the residence times was preceded by the normalization of the mean SUVs from the animals (SUV_A) and human organs to the whole body adult reference male and female phantom weights [14]. This was performed according to (**Equation 1**).

$$\left[\frac{\%}{\text{organ}}\right]_{\text{human}} = SUV_A \times \left(\frac{g_{\text{organ}}}{kg_{\text{weight}}}\right)_{\text{human}} \quad (\textbf{Equation 1})$$

The normalized SUVs were then un-decay corrected to their respective time point. The animal and patient organs and the kidney subregions of the pigs, NHP, and human residence times (MBq-h/MBq) were assessed by trapezoidal approximation of the collected kinetic data, followed by the extrapolation of the remaining points from the last time point to infinity by a single mono-exponential fit. Bone marrow residence times were assessed according to the bone marrow blood model [15]. The remainder of the body residence times for [^{68}Ga]Ga-DO3A-VS-Cys^{40}-Exendin-4 was obtained by taking the theoretical residence time of Gallium-68 minus the total residence times in the source organs, and the difference was assumed to be homogeneously distributed in the body.

Absorbed dose calculations: The estimation of the absorbed dose was performed by OLINDA/EXM 1.1 software where the calculations were based on the adult reference male or female phantom to obtain the intended absorbed dose estimate in humans (ICRP60). The kidney subregion absorbed doses were calculated based on the multi-region kidney model phantom [16].

Results

Comparison of biodistribution of [^{68}Ga]Ga-DO3A-VS-Cys^{40}-Exendin-4 in the different species

In vivo PET imaging: The representative PET images of the normal biodistribution, following the intravenous injection of [^{68}Ga]Ga-DO3A-VS-Cys^{40}-Exendin-4 in pigs, non-human primates, and human are shown in **Figure 1**. In the pigs, non-human primates, and human, the distinct uptake of the tracer in the pancreas could be delineated within 10 minutes post injection (**Figure 1A-C**). These images represent the trans-axial projections of the fused PET-CT images, averaged between 5-15 minutes post injection. The hepatic uptake of the tracer was low and similar to the tracer availability in the blood at later time points in pigs, NHPs and human (**Figure 1D-F**). A high contrast, compared to the hepatic background, is therefore potentially achievable, which is important since the liver is a major site for insulinoma metastasis as well

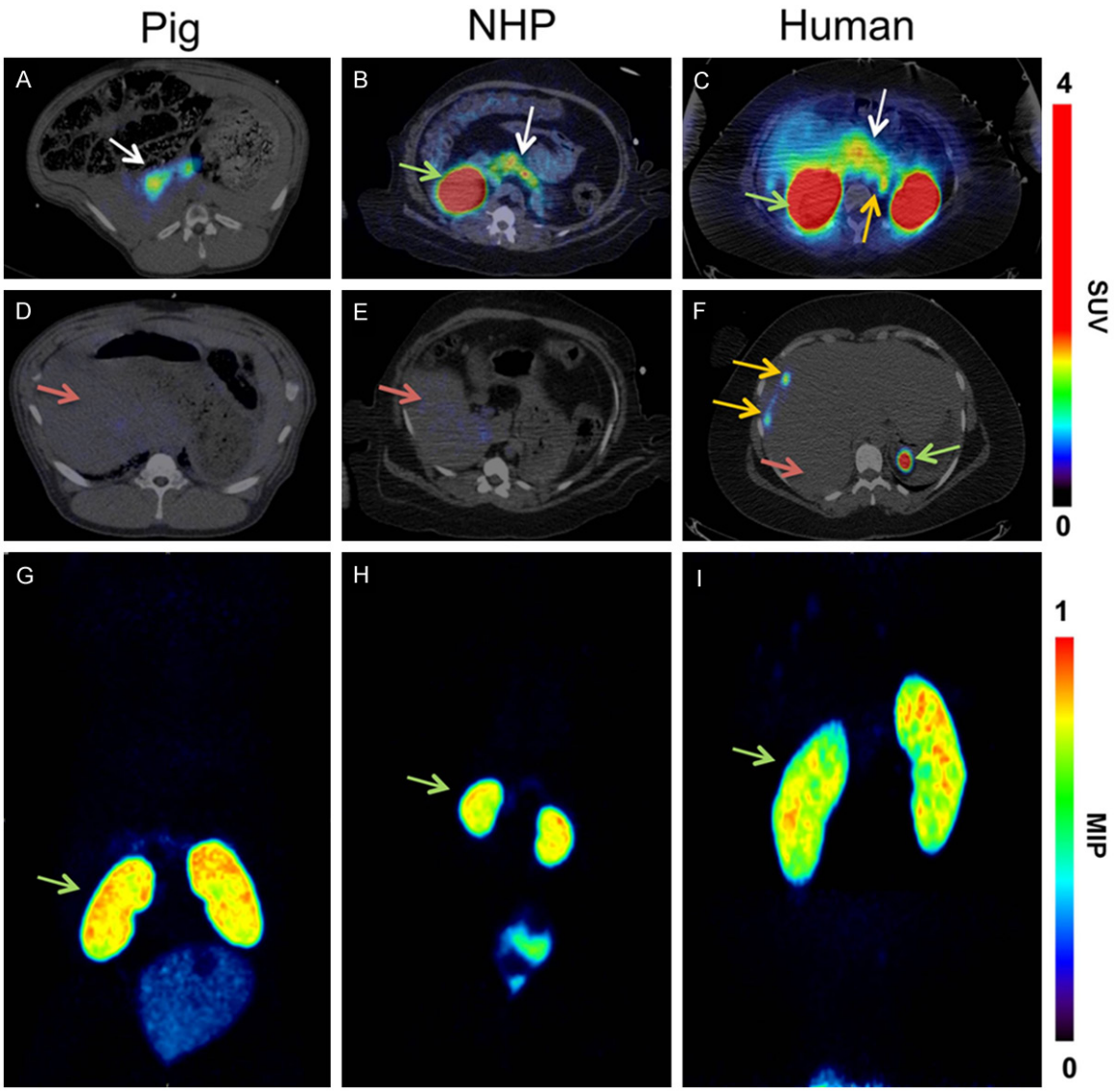

Figure 1. *In vivo* biodistribution of [^{68}Ga]Ga-DO3A-VS-Cys^{40}-Exendin-4 at baseline doses. In vivo biodistribution as analyzed by PET imaging in the pig (0.025 μg/kg; 60 min), NHP (0.01 μg/kg; 90 min), and human (0.17 μg/kg; 40 min, 100 min & 120 min). The pancreas (white arrow) was delineated within 10 minutes post injection in the PET scanner (A-C). The low hepatic uptake (red arrow) of the tracer at baseline (D-F) shows the potential for outlining insulinoma tumor metastasis (F) (orange arrow) and transplanted islets in the liver. The MIP coronal images in demonstrate that the highest uptake of the tracer was observed in the kidneys (green arrow) in all the species (G-I). The color bar for panels (A-F) indicates SUV.

as the clinically relevant recipient organ in islet transplantation. Furthermore, insulinoma metastases in the liver of the patient were clearly visible (**Figure 1F**). The highest accumulation of the tracer was observed in the kidneys; moreover, within the kidney, the accumulation of the tracer was primarily observed in the kidney cortex (**Figure 1G-I**). The coronal images are maximum intensity projections (MIP) of the whole body scan. Apart from the renal excretory organs (kidney and urinary bladder), pancreas, and the insulinoma tumors, no other tissue or organ showed considerable tracer uptake.

Quantification of tracer uptake in the tissue: Organ uptake of [^{68}Ga]Ga-DO3A-VS-Cys^{40}-Exendin-4 in the different species are presented as SUVs in **Figure 2**. Ex vivo organ distribution of [^{68}Ga]Ga-DO3A-VS-Cys^{40}-Exendin-4 in rats showed the highest uptake in the kidney, followed by the spleen, liver, pancreas, heart, and blood (**Figure 2A**). A similar pattern of tracer uptake

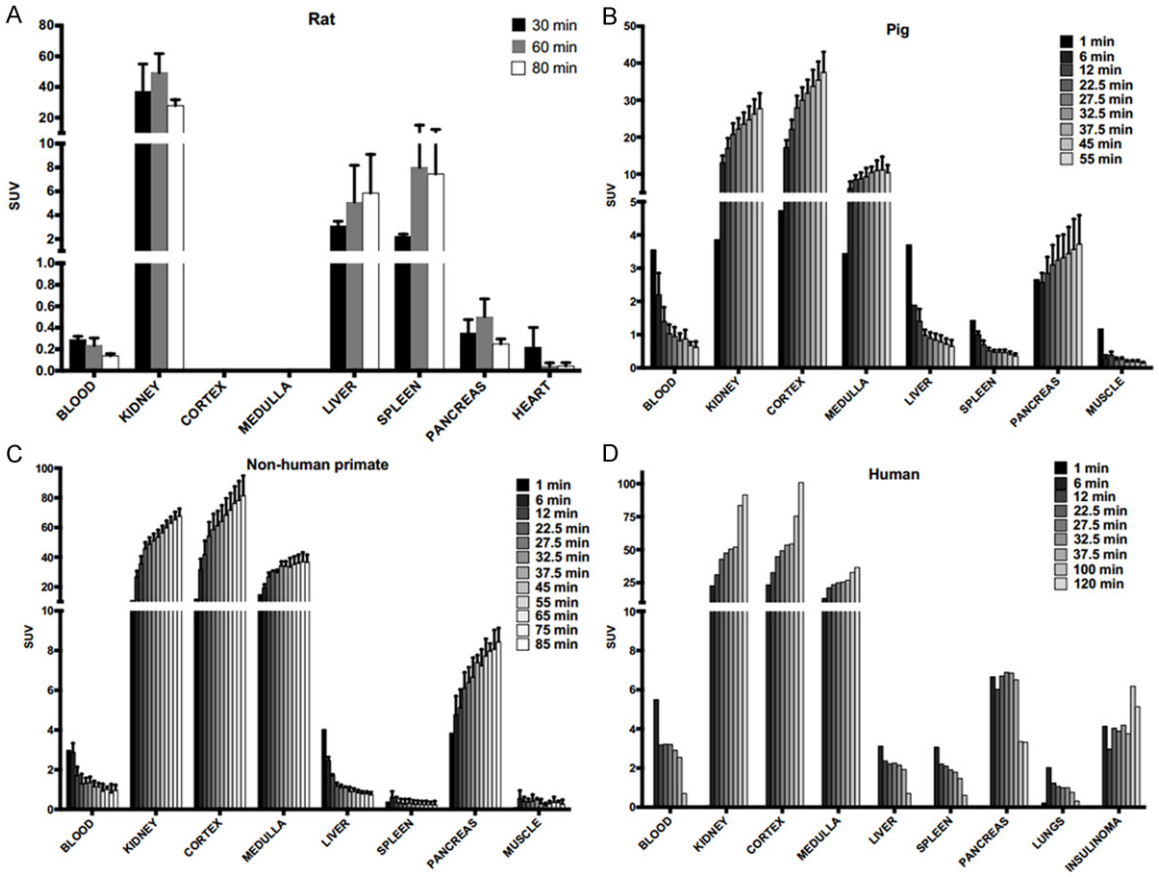

Figure 2. [68Ga]Ga-DO3A-VS-Cys40-Exendin-4 kinetics in the organs of the different species at baseline dose. Rapid clearance of the tracer can be noticed in the blood, liver, and spleen. The tracer uptake in the GLP-1R positive tissue pancreas and the insulinoma tumor increased with time. Retention in the kidneys indicate renal excretion pathway.

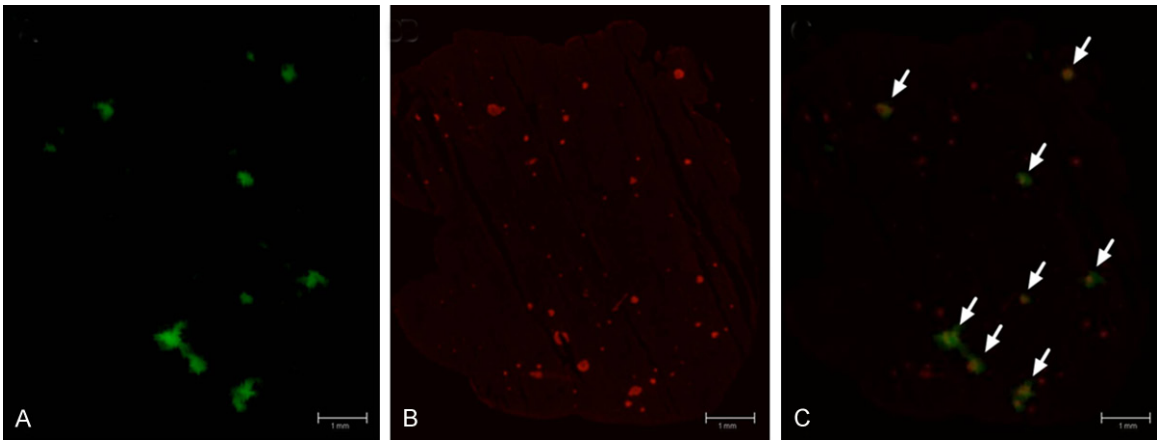

Figure 3. An autoradiogram of rat pancreatic section. (A) The intense areas of radioactive uptake are around 50 times higher than the weak background in the tissue section. The corresponding IF staining for insulin of the same section shows the location of the islets of Langerhans (B). The radioactive distribution of the autoradiogram is highly correlated to the location of the islets of Langerhans, as shown by the autoradiogram/IF stain fusion (C). Only the largest islets are visible in the autoradiogram, but almost no radioactive uptake is found outside of the islets. Scale bar represents 1 mm.

was observed at 30 min, 60 min, and 80 min post injection time points. However, the peak uptake of the tracer in the organs was observed at 60 min post injection. [68Ga]Ga-DO3A-VS-

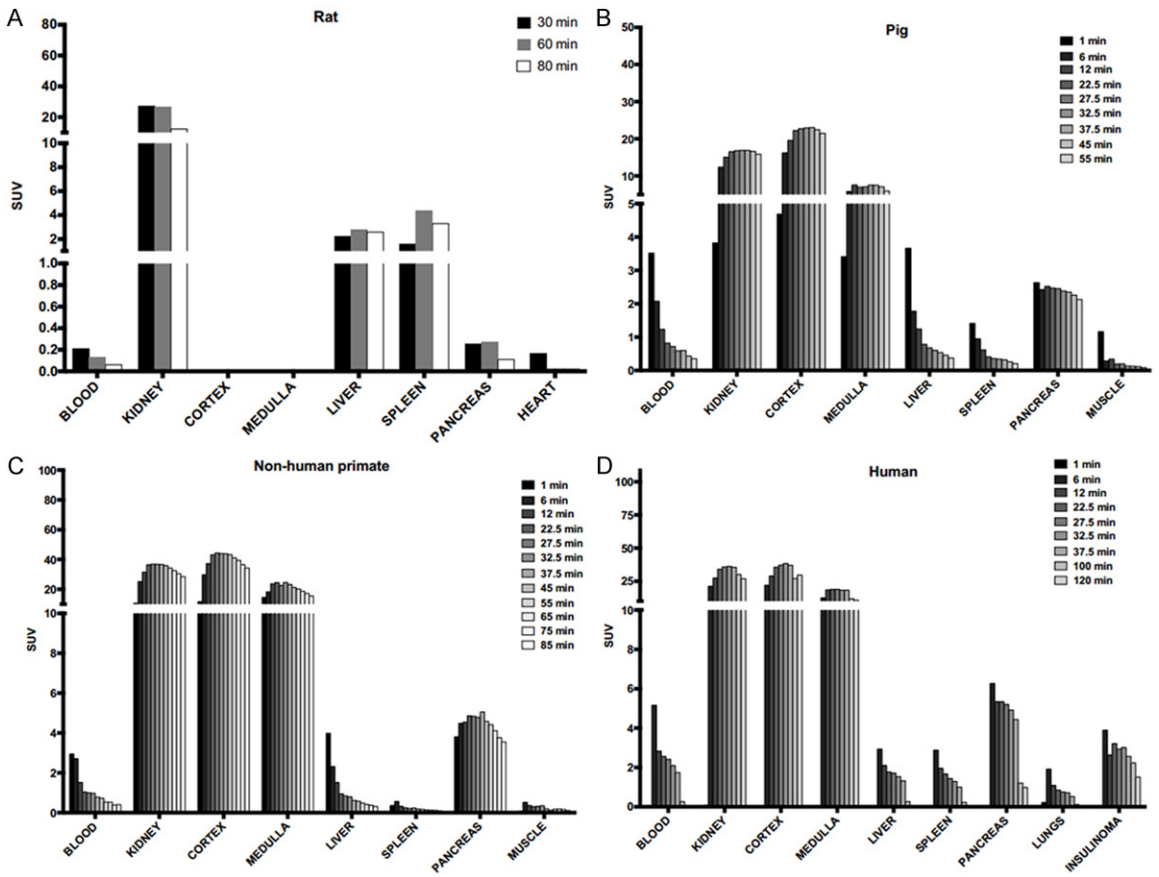

Figure 4. Un-decay corrected kinetics of tracer. The un-decay corrected time-dependent accumulation of [^{68}Ga]Ga-DO3A-VS-Cys^{40}-Exendin-4 which was used for estimating organ residence times in rat (A), pig (B), non-human primate (C) and human patient (D). Actual exposure in all tissues including the kidneys are beginning to decline 30-40 minutes after administration and the assumption of a mono-exponential fit from the last time point to infinity is therefore reasonable.

Cys^{40}-Exendin-4 showed a higher pancreatic and kidney uptake, increasing with time in the pigs, NHP, and in human. At the end of the scan in the patient, the highest uptake of the tracer was quantified in the kidneys, followed by the pancreas and insulinoma tumor (**Figure 2B-D**). Within the kidneys, the cortex showed the highest accumulation increasing with time, with less retention in the kidney medulla. The uptake in the pancreas and insulinoma can be explained by the specific binding to GLP-1R expressed on the beta cells and the tumor. The ex vivo autoradiography study in rats confirmed the heterogeneous distribution of [^{68}Ga]Ga-DO3A-VS-Cys^{40}-Exendin-4 in the pancreas. The focal uptake, corresponding to the islets of Langerhans due to their size and distribution as well as the co-localization between [^{68}Ga]Ga-DO3A-VS-Cys^{40}-Exendin-4 uptake and insulin (**Figure 3A-C**), was more than 48 ± 4 times higher than the weak exocrine background, which has implications for the internal pancreatic radiation dose distribution.

Dosimetry

Residence times were calculated based on the un-decay corrected biodistribution data shown in **Figure 4A-D**. Since there was no apparent uptake in the red marrow, a linear relationship in the blood residence time and the red marrow residence time was assumed to estimate the red marrow radiation dose [15]. The residence times for [^{68}Ga]Ga-DO3A-VS-Cys^{40}-Exendin-4 in the different species, extrapolated to human males and females are shown in **Figure 5**. The organs are presented in decreasing order of residence time, as observed in the patient, with kidney first followed by the muscle, red marrow, liver, pancreas, and spleen. The lung residence time in pigs was not included, as lungs were out

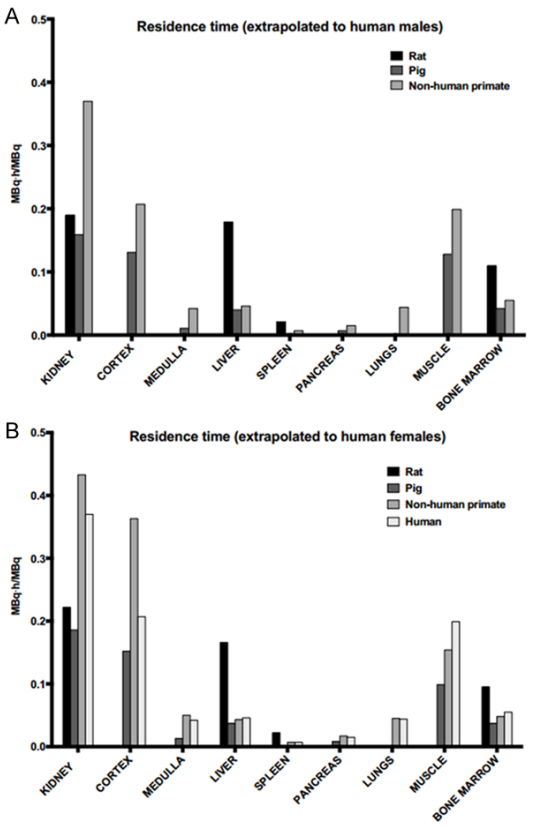

Figure 5. Residence time. Estimated residence times of the tracer at baseline dose in the organs, extrapolated to human from the rat, pig, and NHP; and in a female patient. From the above figure, it is evident that the kidney is the critical organ and the longest residence time in the kidney was observed in the NHP, compared to the other species.

of the field of view during the PET examination. High residence times were observed in the kidney cortex for extrapolations to female and male humans, indicating a trapping of the radionuclide rather than further excretion to the kidney medulla and urinary bladder. Other organs with notable residence times were the muscles, liver, and red marrow for both female and male in all the species.

Table 2 summarizes the estimated doses in human organs, as extrapolated from the different species. The organs are presented in decreasing order of radiation doses observed in the human patient, with kidneys on top followed by the pancreas, red marrow, spleen, liver, muscle, and lung. Hence, the highest radiation dose was observed in the kidneys.

The estimated effective dose, from rat's data, was relatively higher compared to other animal models while it was similar in pigs, non-human primates, and in the patient.

From **Table 2** it is evident that the local dose to the kidney was the limiting factor rather than the estimated whole body effective dose. The kidney dose, extrapolated from the different species, was 0.34 ± 0.06 (rats), 0.28 ± 0.05 (pigs), 0.65 ± 0.1 (NHP), and 0.28 (human) mGy/MBq, which corresponded to the maximum yearly administered amounts of 455 (rat), 536 (pig), 231 (NHP), and 536 (human) MBq before reaching the cut-off value of 150 mGy in the kidney [17].

Discussion

Here, we have estimated the human dosimetry of [^{68}Ga]Ga-DO3A-VS-Cys^{40}-Exendin-4, in order to investigate if repeated imaging examinations are possible before reaching the whole body and organ absorbed dose limits.

The pharmaco-kinetics of [^{68}Ga]-DO3A-VS-Cys^{40}-Exendin-4 in the different species showed a rapid washout from blood and most tissues, but a high retention in the kidneys, followed by specific uptake in the GLP-1R positive tissues such as the pancreas and in the insulinoma (**Figure 2**). Validation of the target specific uptake of [^{68}Ga]Ga-DO3A-VS-Cys^{40}-Exendin-4 in these tissues has been published previously [3, 4, 6]. The long residence times in the kidneys are most likely due to tubular reabsorption, predicting a high absorbed radiation dose, which makes these organs critical. The estimated absorbed dose in the kidney ranged between 0.30-0.73 mGy/MBq for females and 0.26-0.42 mGy/MBq for males, extrapolated from all the species (**Table 3**). Among the different species, the highest absorbed dose was observed in the NHP. In the patient study, the most relevant for the clinical situation, the absorbed dose in the kidney was 0.28 mGy/MBq.

Given a yearly acceptable kidney dose of 150 mGy, this compares to approximately 536 and 231 MBq of administered tracer per year based on the clinical data and the extrapolation from the NHP, respectively. We have previously shown that the administration of more than 0.1 μg/kg of aExendin-4 peptide induces a partial saturation of the GLP-1R [3]. Assuming a routinely reproducible specific radioactivity of 50 MBq/nmol, which is reasonable for modern ^{68}Ga/^{68}Ge generators and based on previous

Table 2. Estimated absorbed dose of the tracer at baseline dose in the organs and effective dose in the different species

Gallium-68 absorbed Doses (mGy/MBq)							
Organ	Rat		Pig		NHP		Patient
Extrapolated to human	Female	Male	Female	Male	Female	Male	Female
Kidneys	0.375	0.296	0.314	0.248	0.725	0.571	0.276
Kidney Cortex	N/A	N/A	0.303	0.261	0.729	0.420	0.378
Kidney Medulla	N/A	N/A	0.124	0.106	0.390	0.298	0.181
Pancreas	0.014	0.011	0.051	0.040	0.102	0.080	0.050
Red Marrow	0.027	0.029	0.022	0.021	0.022	0.022	0.026
Spleen	0.075	0.060	0.015	0.012	0.034	0.026	0.023
Liver	0.065	0.052	0.019	0.015	0.022	0.018	0.022
Muscle	0.013	0.011	0.008	0.006	0.009	0.007	0.015
Lungs	0.014	0.011	0.014	0.011	0.030	0.024	0.013
Effective dose (mSv/MBq)	0.02	0.014	0.017	0.011	0.018	0.013	0.016

Table 3. Comparison of dosimetry of other reported exendin-4 radiotracers. Doses are given as mGy/MBq unless otherwise stated

Organ	[^{68}Ga]Ga-DO3A-VS-Cys^{40}-Exendin-4 [human data, **Table 2**]	[Lys^{40}(Ahx-DOTA-^{111}In) NH2]-exendin-4 [18]	[Lys^{40}(AhxHYNIC-^{99m}Tc/EDDA)NH2]-exendin-4 [19]	[^{64}Cu]NODAGA-exendin-4 [20]
Kidney	0.276	4.48	0.083	1.48
Liver	0.022	0.20	0.0046	N/A
Lungs	0.013	0.13	0.0046	N/A
Pancreas	0.050	0.70	0.020	N/A
Muscles	0.015	0.12	0.0024	N/A
Bone marrow	0.026	0.14	0.0030	N/A
Spleen	0.023	0.37	0.068	N/A
Effective dose (mSv/MBq)	0.016	0.155	0.0037	0.074

N/A: information not available.

radiosynthesis of this tracer, then 50-100 MBq at most can be administered to a subject of 73 kg in order to keep below 0.1 μg/kg administered peptide. Thus, at least 5-10 (clinical data) or 2-4 (NHP extrapolation) examinations can potentially be performed yearly in humans.

The estimated whole body effective dose was similar, regardless of species differences and was at most 0.020 μSv/MBq (extrapolated from rat). Administration of 50-100 MBq of [^{68}Ga]Ga-DO3A-VS-Cys^{40}-Exendin-4 would yield a dose of 1-2 mSv. A CT examination for anatomical information and attenuation correction amounts to approximately 1 mSv per bed position, and when added to the PET dose, it gives a total of 2-3 mSv per examination. This corresponds to 3-5 PET/CT examinations yearly before reaching the acceptable whole body dose of 10 mSv. With the potential increasing use of hybrid PET/MR scanners in the future, the additional radiation dose from the anatomical examination is null and can be disregarded.

In comparison with other reported Exendin-4 analogues, labeled with other radiometals, we observed that the extrapolated absorbed dose of [^{68}Ga]Ga-DO3A-VS-Cys^{40}-Exendin-4 is lower (**Table 3**). The absorbed dose in kidney for Indium-111 and Copper-64 labeled Exendin-4 was approximately 17and 5 times that of [^{68}Ga]Ga-DO3A-VS-Cys^{40}-Exendin-4, respectively [18]. Furthermore, the absorbed doses in all the other organs were relatively lowest for [^{68}Ga]Ga-DO3A-VS-Cys^{40}-Exendin-4 except for the Technicium-99m labeled Exendin-4 [19]. The extrapolated effective doses ranging from 0.016-0.02 mSv/MBq and 0.011-0.014 mSv/MBq for human females and males, respectively, were also lower compared to the other Exendin-4 labels. For instance, the effective dose for Indium-111and Copper-64 labeled Exendin-4 was10 and 5 times higher, respectively,

than the effective dose of [^{68}Ga]Ga-DO3A-VS-Cys^{40}-Exendin-4 [20].

Recently, several Fluorine-18 labeled analogues of Exendin-4 have been developed [21, 22]. Some have a significantly lower renal retention with a correspondingly lower kidney radiation dose [23]. The potential drawback may instead be a higher whole body effective dose due to the relative longer half-life of Fluorine-18 (109.8 minutes) compared to Gallium-68. The dosimetry of Fluorine-18 labeled Exendin-4 has not yet been reported to the authors' knowledge.

The *ex vivo* examination of the pancreas in rats reveals that the uptake was highly focal rather than homogenous. This is not surprising and has been shown previously for radiolabeled Exendin-4 analogues. It has important implications for the estimation of tissue radiation dose, since the models are programmed to assume a homogenous tissue distribution. Thus, the rather insignificant pancreatic dose calculated here actually corresponds to a higher dose to selected areas of the pancreas. These areas are identical to the islets of Langerhans and their beta cells, which are known to have high expression of GLP-1R [24]. The autoradiography study showed a 50-fold higher uptake in these areas, compared to the remaining exocrine pancreas. Naively, this may be extrapolated to yield a 50 times higher radiation dose, potentially approaching doses which may harm the beta cells and cause diabetogenic effects. However, the Full Width Half Maximum (FWHM) range of the positron emitted from Gallium-68 is in excess of 500μm, before annihilation due to its relatively high energy (E_{max}=1900 keV) [25]. Therefore, the deposited dose will not be concentrated solely inside the islets of Langerhans, which have a diameter of 8-500 μm (mean 150 μm). In contrast, the local dose to the islets of Langerhans will be substantially higher for the positron emitting nuclides with a shorter range (such as Fluorine-18, FWHM=100 μm, E_{max}=635 keV), as well as for the imaging nuclides with a fraction of other modes of emission (for example, Indium-111 auger electrons). In fact, Indium-111 labeled Exendin-4 was previously shown to ablate insulin producing INS-1 cells in mice when given in sufficient doses [26]. We, therefore, speculate that the risk is low for diabetogenic effects due to the locally deposited radiation dose in the islets of Langerhans for Gallium-68, especially compared to other available radionuclides used for Exendin-4 based imaging.

Conclusion

Here, we show that [^{68}Ga]Ga-DO3A-VS-Cys^{40}-Exendin-4 can be administered repeatedly (2-4) per year in human without exceeding the radiation limits in criticial organ, kidney or from estimated effective dose. This potentially enables longitudinal diagnostic studies not only in insulinoma patients but also in other populations such as subjects developing T1D/T2D, subjects with transplanted islet grafts as well as healthy volunteers enrolled in the early phase of drug development studies.

Acknowledgements

Olof Eriksson's position was supported by ExoDiab. Ram Kumar Selvaraju's position was supported by the Barndiabetesfonden and Diabetesfonden. Thomas N. Bulenga was supported by the Swedish Institute Scholarship.

Disclosure of conflict of interest

None.

Address correspondence to: Ram Kumar Selvaraju, Department of Medicinal Chemistry, Preclinical PET Platform (PPP), Uppsala University, Box 574, SE-751 83 Uppsala Sweden. Tel: +46-704-122188; +46-18-4715304; Fax: +46-18-4715307; E-mail: ramkumar.selvaraju@pet.medchem.uu.se

References

[1] Marinelli LD, Quimby EH, Hine GJ. Dosage determination with radioactive isotopes; practical considerations in therapy and protection. Am J Roentgenol Radium Ther Nucl Med 1948; 59: 260-81.

[2] Quimby E, Feitelberg S. Radioactive isotopes in medicine and biology. Philadelphia: Lea and Febiger; 1963.

[3] Selvaraju RK, Velikyan I, Johansson L, Wu Z, Todorov I, Shively J, Kandeel F, Korsgren O, Eriksson O. In Vivo Imaging of the glucagon-like peptide 1 receptor in the pancreas with ^{68}Ga-labeled DO3A-exendin-4. J Nucl Med 2013; 54: 1458-63.

[4] Nalin L, Selvaraju RK, Velikyan I, Berglund M, Andréasson S, Wikstrand A, Rydén A, Lubberink M, Kandeel F, Nyman G, Korsgren O, Eriksson O, Jensen-Waern M. Positron emission tomography imaging of the glucagon like peptide-1 receptor in healthy and streptozoto-

cin-induced diabetic pigs. Eur J Nucl Med Mol Imaging 2014; 41: 1800-10.
[5] Eriksson O, Velikyan I, Selvaraju RK, Kandeel F, Johansson L, Antoni G, Eriksson B, Sörensen J, Korsgren O. Detection of metastatic insulinoma by positron emission tomography with [^{68}Ga]Exendin-4 - a case report. J Clin Endocrinol Metab 2014; 99: 1519-24.
[6] Selvaraju RK, Velikyan I, Asplund V, Johansson L, Wu Z, Todorov I, Shively J, Kandeel F, Eriksson B, Korsgren O, Eriksson O. Pre-clinical evaluation of [^{68}Ga]Ga-DO3A-VS-Cys^{40}-Exendin-4 for imaging of insulinoma. Nucl Med Biol 2014; 41: 471-6.
[7] World Health Organization. Definition, diagnosis and classification of diabetes mellitus and its complications: report of a WHO consultation, 1999.
[8] Stang J, Story M (eds). Diabetes Mellitus: Type 1 and Type 2. Guidelines for adolescent nutrition services (2005) http://www.epi.umn.edu/let/pubs/adol_book.shtm 2000; 12(2).
[9] Körner M, Stöckli M, Waser B, Reubi JC. GLP-1 receptor expression in human tumors and human normal tissues: potential for in vivo targeting. J Nucl Med 2007; 48: 736-43.
[10] Jensen RT, Gibril F and Termanini B. Definition of the role of somatostatin receptors scintigraphy in gastrointestinal neuroendocrine tumor localization. Yale J Biol Med 1997; 70: 481-500.
[11] Stabin MG, Sparks RB, Crowe E. OLINDA/EXM: The second-generation personal computer software for internal dose assessment in nuclear medicine. J Nucl Med 2005; 46: 1023-1027.
[12] Velikyan I, Beyer GJ, LångströmB. Microwave-supported preparation of ^{68}Ga bioconjugates with high specific radioactivity. Bioconjug Chem 2004; 15: 554-560.
[13] Velikyan I, Xu H, Nair M, Hall H. Robust labeling and comparative preclinical characterization of DOTA-TOC and DOTA-TATE. Nucl Med Biol 2012; 39: 628-639.
[14] Cristy M, Eckerman K. Specific absorbed fractions of energy at various ages from internal photons sources. ORNL/TM-8381 V1-V7. Oak Ridge National Laboratory, Oak Ridge, TN, 1987.
[15] Sgouros G. Bone marrow dosimetry for radioimmunotherapy: theoretical considerations. J Nucl Med 1993; 34: 689-694.
[16] Bouchet LG, Bolch WE, Blanco HP, Wessels BW, Siegel JA, Rajon DA, Clairand I, Sgouros G. MIRD Pamphlet No. 19: Absorbed fractions and radionuclide S values for six age-dependent multiregion models of the kidney. J Nucl Med 2003; 44: 1113-1147.
[17] http://www.euronuclear.org/info/encyclopedia/r/radiation-exposure-dose-limit.htm.
[18] Wild D, Wicki A, Mansi R, Béhé M, Keil B, Bernhardt P, Christofori G, Ell PJ, Mäcke HR. Exendin-4–Based Radiopharmaceuticals for glucagon-like peptide-1 receptor PET/CT and SPECT/CT. J Nucl Med 2010; 51: 1059-1067.
[19] Tomaszuk M, Sowa-Staszczak A, Lenda-Tracz W, Glowa B, Pach D, Buziak-Bereza M, et al. Dosimetry of exendin-4 based radiotracer for glucagon-like peptide-1 receptor imaging: an initial report. J Phys Conf Ser 2011; 317: 012011.
[20] Mikkola K, Yim CB, Fagerholm V, Ishizu T, Elomaa VV, Rajander J, Jurttila J, Saanijoki T, Tolvanen T, Tirri M, Gourni E, Béhé M, Gotthardt M, Reubi JC, Mäcke H, Roivainen A, Solin O, Nuutila P. ^{64}Cu- and ^{68}Ga-labelled [Nle(14), Lys(^{40})(Ahx-NODAGA)NH2]-exendin-4 for pancreatic beta cell imaging in rats. Mol Imaging Biol 2014; 16: 255-63.
[21] Wu Z, Liu S, Hassink M, Nair I, Park R, Li L, Todorov I, Fox JM, Li Z, Shively JE, Conti PS, Kandeel F. Development and evaluation of ^{18}F-TTCO-Cys^{40}-Exendin-4: a PET probe for imaging transplanted islets. J Nucl Med 2013; 54: 244-51.
[22] Kiesewetter DO, Guo N, Guo J, Gao H, Zhu L, Ma Y, Niu G, Chen X. Evaluation of an [^{18}F]AlF-NOTA Analog of exendin-4 for imaging of GLP-1 receptor in insulinoma. Theranostics 2012; 2: 999-1009.
[23] Mikkola K, Yim CB, Lehtiniemi P, Elomaa VV, Ishizu T, Rajander J, et al. Towards clinical imaging With ^{18}F-labelled exendin-4, synthesized via click chemistry. Abstract. American Diabetes Association.
[24] Tornehave D, Kristensen P, Romer J, Knudsen LB, Heller RS. Expression of the GLP-1 receptor in mouse, rat, and human pancreas. J Histochem Cytochem 2008; 56: 841-51.
[25] Levin CS, Hoffman EJ. Calculation of positron range and its effect on the fundamental limit of positron emission tomography system spatial resolution. Phys Med Biol 1999; 44: 781-799.
[26] Wicki A, Wild D, Storch D, Seemayer C, Gotthardt M, Behe M, Kneifel S, Mihatsch MJ, Reubi JC, Mäcke HR, Christofori G. [Lys40(Ahx-DTPA-^{111}In)NH_2]-Exendin-4 is a highly efficient radiotherapeutic for glucagon-like peptide-1 receptor-targeted therapy for insulinoma. Clin Cancer Res 2007; 13: 3696-705.